Flight Trials of the Wide-Area Augmentation System (WAAS)

T. Walter, C. Kee, Y.C. Chao, Y.J. Tsai, U. Peled, J. Ceva, A. K. Barrows, E. Abbott, D. Powell, P. Enge, and B. Parkinson

Stanford University
September 23rd, 1994

BIOGRAPHIES

The authors are presently at Stanford University where their research concentrates on all aspects of the Wide-Area Augmentation System. Since November of 1993 the group has been primarily focused on putting together and evaluating a functioning real-time Wide-Area Differential network.

ABSTRACT

The Wide-Area Augmentation System (WAAS) is being rapidly developed by the Federal Aviation Administration for supplemental operational use in 1997. In time, it will be a primary navigation aid for all phases of flight down to Category I precision approach. The WAAS will include a network of approximately 20 to 30 Wide-area Reference Stations (WRSs) distributed around the National Airspace System. These reference stations will observe all GPS satellites in view and send pseudorange and ionospheric observations back to one or more Wide-area Master Stations (WMSs). The WMSs will use this data to form *vector* corrections for each GPS satellite. These vectors contain separate components for the satellite ephemeris, satellite clock and ionosphere. The corrections will be broadcast to WAAS users via a geostationary satellite, using a signal and data format, which has been designed by RTCA Special Committee 159.

In the Summer of 1994, Stanford performed WAAS flight trials to provide WAAS operational experience as early as possible. Our flight trials used three WAAS Reference Stations (WRSs), which Stanford installed for the FAA in the Western United States. They also used an experimental WMS located at Stanford. The flights used Professor David Powell's Piper Dakota to fly WAAS precision approaches to an uninstrumented airport (Palo Alto). The WAAS data dramatically improved the accuracy of the airborne GPS fix, and it drove an "ILS-like" display. This paper describes our experiment and reports the results of the flights.

1 INTRODUCTION

In time, the Global Positioning System will be used for a wide variety of aircraft operations. However, aircraft use of any satellite-based navigation system raises significant concern with respect to integrity (all hazardous position errors are detected), reliability (continuity of service), time availability and accuracy. A single satellite malfunction would affect users over a huge geographic area. A navigation system with integrity warns its users if position errors may be greater than a pre-specified "alarm limit."

The integrity requirement for any navigation system depends on whether it is the primary navigation aid or supplements another system. If the radionavigation system is supplemental, then it must detect signal failures with high probability. However, the time availability of these "guaranteed" position fixes is not a crucial concern, because another system is presumably available. A primary radionavigation system must deliver these fault free position fixes with a time availability in excess of 0.999 (Category I approach) or 0.99999 (enroute, terminal, and non-precision approach phases of flight).

The Wide-Area Augmentation System (WAAS) is a safety-critical navigation system that adds a signal-in-space and an independent ground network to the Global Positioning System (GPS). When first operational in 1997, it will be a supplemental system for enroute through precision approach air navigation. In time, it will become a primary navigation sensor. The WAAS will augment GPS with the following three services: a ranging function which improves availability and reliability; differential GPS corrections which improve accuracy; and integrity monitoring which improves safety.

The WAAS concept is shown in Figure 1. As shown, it broadcasts GPS integrity and correction data to GPS users and also provides a ranging signal that augments GPS. At present, a test WAAS signal is

being broadcast from the geostationary Inmarsat-2 satellite over the western portion of the Atlantic (AOR-W). This test signal has been used to broadcast differential corrections and integrity information. It has not yet been used as a ranging signal [5]. By 1996 or 1997, the WAAS signal will be broadcast to users from the geostationary Inmarsat-3 satellites.

The WAAS ranging signal will be "GPS-like" and will be received by slightly modified GPS receivers. More specifically, it will be at the GPS L_1 frequency (or near L_1) and will be modulated with a spread spectrum code from the same family as the GPS C/A codes. The code phase and carrier frequency of the signal will be controlled such that the WAAS satellites will provide additional range measurements to the GPS user. As mentioned earlier, the WAAS signal will also carry data that contains differential corrections and integrity information for all GPS satellites as well as the geostationary satellite(s).

The ground network shown in Figure 1 develops the differential corrections and integrity data which is broadcast to the users. Wide-area Reference Stations (WRSs) are widely dispersed data collection sites that receive and process signals received from the GPS and geostationary satellites. For example, a network concept for the United States is shown in Figure 2. The WRSs forward their data to data processing sites referred to as Wide-area Master Stations (WMSs or central processing facilities).

The WMSs process the raw data to determine integrity, differential corrections, residual errors, and ionospheric delay information for each monitored satellite. They also develop ephemeris and clock information for the geostationary satellites. All this data is packed into the WAAS message, which is sent to Navigation Earth Stations (NESs). The NESs uplink this message to the geostationary satellites

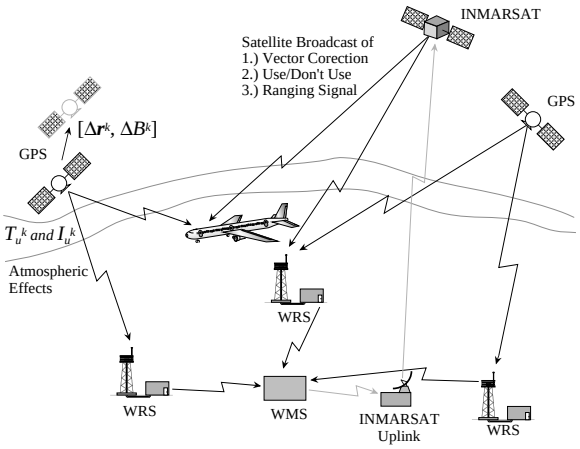

Figure 1 *The Wide-Area Augmentation System is shown here.*

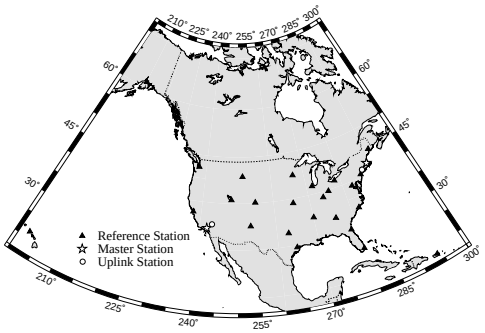

Figure 2 *This figure shows an example WAAS ground network for the United States*

which broadcast the "GPS-like" signal described earlier. Taken together, the differential corrections and the improved geometry provided by the geostationary satellites will improve user accuracy to better than 10 meters (2drms) in the vertical, which is adequate for aircraft Category I precision approach. The integrity data will improve user safety by flagging GPS satellites that are behaving incorrectly and cannot be corrected. In fact, the WAAS can deliver health warnings to the pilot within 6 seconds of a GPS satellite malfunction.

Our experimental WAAS testbed is a precursor of the final WAAS network and is described in Sections 2, 3, 4 and 5 of this paper. This testbed was constructed by Stanford University and is funded by the Satellite Program Office (AGS-100) of the Federal Aviation Administration. It is used to develop early operational experience with the WAAS and for the development and test of new WAAS algorithms. As shown in Figure 3, it includes Wide-Area Reference Stations (WRSs) located at Elko, Nevada, San Diego and Arcata, California. The data from each of these three stations is sent back to the Wide-area Master Station (WMS) at Stanford University. The WMS forms the RTCA SC 159 WAAS message, which is sent to the aircraft using a UHF radio.

The Wide-area Reference Station (WRS) algorithms are detailed in Section 2. This algorithm develops slant range ionospheric delay estimates as well as "iono-free," "tropo-free" pseudorange residuals. This raw data is sent via phone lines from the WRSs to the WMS at Stanford University.

Our WMS is described in Section 3. It contains an algorithm for the development of ionospheric corrections from the ionospheric delay estimates, and a separate algorithm to estimate the GPS ephemeris and clock errors from the pseudorange residuals. As described in Section 3, the WMS forms a vector correction (ionosphere, satellite clock and satellite ephemeris), which is packed into the WAAS message

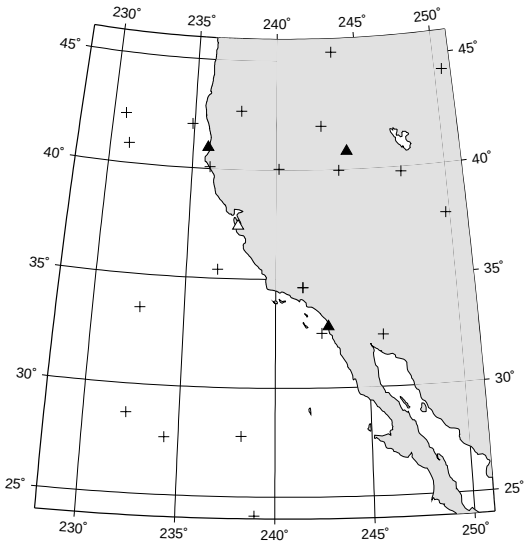

Figure 3 *Three WRSs are shown on this map (black triangles) as well as the location of the master station (white triangle). Also shown are the locations of the ionospheric pierce points (+) of the WRSs for one instant in time.*

format designed by Working Group 2 of RTCA SC 159 [4] [11].

The data link and format are described in Section 4. The data link is a cascade of a telephone link and a UHF radio. The telephone connects the WMS on campus to any site near the flight trials. The UHF radio connects the ground site to Professor David Powell's Piper Dakota, which is our test aircraft. As such, it provides the wireless connection over the "last mile" to the aircraft. In fact, its range is ten or more miles depending on obstructions. In the future, we will use the Inmarsat satellites in the Pacific Ocean Region (POR) to provide the connection to the test aircraft.

The WAAS avionics are described in Section 5. These include the UHF receiver, a computer which converts and applies the WAAS correction, the GPS receiver, and the pilot displays.

Our test results are described in Section 6. These include static results measured with a GPS receiver at a known location on the Stanford campus. They also include flight results from Palo Alto airport. For the flight trials, the known altitude of the runway is the truth source.

A brief summary is given in Section 7.

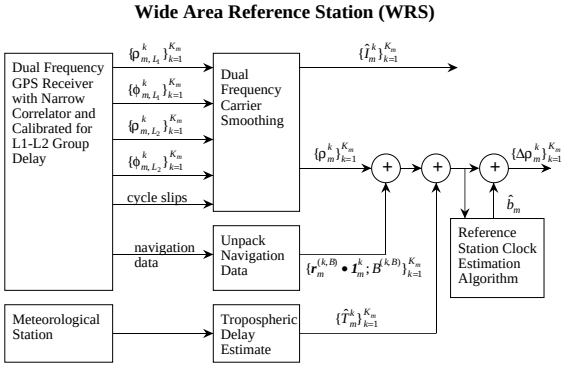

Figure 4 *Shows a schematic diagram of the components and processes of the WRS.*

2 WIDE AREA REFERENCE STATIONS

Our WRS is shown in Figure 4. It uses a dual frequency (cross-correlating) receiver to produce code and carrier phase observations at L_1 and L_2. The set of code observations at L_1 and L_2 are denoted $\{\rho^k_{m,L_1}\}_{k=1}^{K_m}$ and $\{\rho^k_{m,L_2}\}_{k=1}^{K_m}$ respectively, where K_m are the number of satellites in view of the m^{th} reference station. Similarly, the set of carrier phase observations at L_1 and L_2 are denoted $\{\phi^k_{m,L_1}\}_{k=1}^{K_m}$ and $\{\phi^k_{m,L_2}\}_{k=1}^{K_m}$, respectively. These carrier phase observations at the two frequencies are used to smooth the code phase observations and to produce estimates of the slant ionospheric delay between the reference station and the satellites.

The outputs of the carrier smoothing algorithm are: smoothed pseudorange estimates which are free of ionospheric delays $\{\rho^k_m\}_{k=1}^{K_m}$, and the ionospheric delay estimates $\{I^k_m\}_{k=1}^{K_m}$. These smoothed pseudorange estimates are well modeled by

$$\rho^k_m = \left(\left|\boldsymbol{r}^k_m\right| + b_m - B^k\right) + \Delta I^k_m + T^k_m + \nu^k_m$$
$$\approx \left(\left|\boldsymbol{r}^k_m\right| + b_m - B^k\right) + T^k_m + \nu^k_m$$

where the second line assumes that the ionospheric error term is small enough to be included in the noise term.

Then, the reference station subtracts the nominal range to the satellite (as computed from the data in the satellite navigation message and the known location of the reference station) from the measured pseudorange. It further reduces the pseudorange estimate by the nominal satellite clock offset as described by the clock field in the navigation message. These reduced pseudoranges are given by

$$\Delta\rho_m^k = \left|\boldsymbol{r}_m^k\right| - \left|\boldsymbol{r}_m^{(k,B)}\right| + b_m - \left(B^k - B^{(k,B)}\right) + T_m^k + \nu_m^k$$
$$\approx \Delta\boldsymbol{r}^k \bullet \boldsymbol{1}_m^k + b_m - \left(B^k - B^{(k,B)}\right) + T_m^k + \nu_m^k$$
$$= \Delta\boldsymbol{r}^k \bullet \boldsymbol{1}_m^k + b_m - \Delta B^k + T_m^k + \nu_m^k$$

where $\Delta\boldsymbol{r}^k$ is the vector which connects the true location of the satellite, $\boldsymbol{r}^k$, and the location of the satellite according to the navigation message, $\boldsymbol{r}^{(k,B)}$. In the above, $\boldsymbol{1}_m^k$ denotes the unit vector from the k^{th} satellite towards the m^{th} reference station. Additionally, B^k is the true offset of the satellite transmission from GPS time, and $B^{(k,B)}$ is the offset according to the navigation message.

Next, the reference station subtracts an estimate of the tropospheric delay from the observed pseudorange. Importantly, the tropospheric estimate is not based on elevation angle alone. Rather, it is based on elevation angle *and* local measurements of pressure, temperature and humidity. Indeed, a model without this side information can suffer errors of 2 meters for satellites at low elevation angles. In contrast, a model with the surface measurements does not usually have errors greater than 30 centimeters.

Finally, the reference station of Figure 4 uses a "clock steering" algorithm to estimate the reference station clock offset. This algorithm averages the reduced pseudoranges from all of the satellites in view to form an estimate of the reference station clock. This averaging reduces the erroneous contribution due to the individual satellite clock and ephemeris errors as well as the pseudorange measurement noise. In addition, if the reference station has a high quality clock such as a Rubidium oscillator, then the WRS clock estimates can be averaged over time to further reduce the clock estimate error. This averaging strategy prevents numerical overflow in the data to be sent to the central site. It also yields pseudorange error estimates which are approximate but physically meaningful at the reference station. However, it can also introduce jumps in the clock estimates when the set of satellites in view changes. This possibility must be correctly taken into account.

The reference station clock estimates are subtracted from the smoothed pseudoranges to yield

$$\Delta\rho_m^k = \Delta\boldsymbol{r}^k \bullet \boldsymbol{1}_m^k + \Delta b_m - \Delta B^k + \nu_m^k$$

As shown in Figure 4, these pseudorange residuals (for all the satellites in view) are sent along with the vertical ionospheric delay estimates, $\{\boldsymbol{I}_m^k\}_{k=1}^{K_m}$, to the central site for processing.

Wide Area Master Station (WMS)

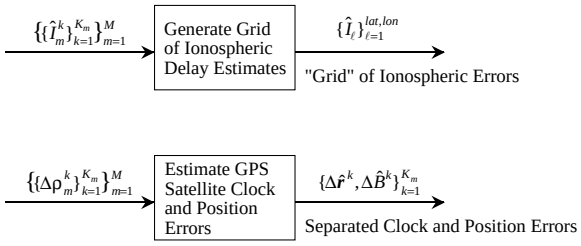

Figure 5 *The two main functions of the WMS are depicted here.*

3 WIDE AREA MASTER STATION

The WMS algorithms are shown in Figure 5. The WMS processes the ionospheric delay data from the WRS to generate a "grid" of ionospheric delay estimates. In a separate procedure, it uses the "iono- and tropo-free" pseudorange residuals to estimate the clock and ephemeris errors for each satellite in view of the network. Only the ionospheric algorithm is described in this paper.

The WMS receives the following ionospheric data from the *M* reference stations

$$\{\{\boldsymbol{I}_m^k\}_{k=1}^{K_m}\}_{m=1}^{M}$$

The literature has described at least two ways to process such data to yield a regional model of the ionosphere.

As described in [6], this data can be used to form a maximum likelihood estimate of the parameters in the single frequency ionospheric model. These estimates may be found using Newton's method, and would significantly increase the accuracy of a single frequency user's ionospheric estimate.

Another option is described in [3] and [8]. Here the ionospheric data from the reference stations could be used to form a grid of ionospheric estimates. The user could interpolate between the grid points and once again realize a substantial improvement in accuracy. This "grid" algorithm is used in the current version of our WMS, and it operates as follows:

1. The WRSs measure the slant ionospheric delays to all satellites in view. These delays are measured over a widely dispersed set of "pierce points." For example, the pierce points at one instant of time for Stanford's experimental network are shown in Figure 3. This set of data is the input to the ionospheric processing algorithms.

2. The WRSs convert the slant ionospheric delays to vertical delay estimates by dividing by the following scale factor:

$$SF = \frac{1}{\sin(El_p)} = \frac{1}{\sqrt{1-\left(\frac{r_e \cos(El_r)}{r_e + h_m}\right)^2}}$$

where El_p is the local elevation angle at the pierce point, El_r is the elevation angle at the WRS, r_e is the average radius of the earth, and h_m is the height of the maximum electron density (assumed to be 350 km).

3. The WRSs send the vertical ionospheric delays to the WMS.

4. The WMS uses the WRS data to form a grid of vertical ionospheric grid estimates. This grid may be uniform in latitude and longitude with points every 5 degrees. The estimated vertical delays for every grid point are given by [3]

$$I^{j}_{WDGPS,V} = I^{j}_{Klo,V}\left[\sum_{k=1}^{K}\left(\frac{I^{k}_{Meas,V}}{I^{k}_{Klo,V}}\right)\frac{1/d_{k,j}}{\sum_{n=1}^{K} d_{n,j}}\right]$$

where $I^{j}_{WDGPS,V}$ is the WDGPS estimate for the j^{th} grid point. Additionally, $I^{j}_{Klo,V}$ is the ionospheric estimate for the j^{th} grid point using the Klobuchar single frequency model, $I^{k}_{Meas,V}$ is the WRS measurement for the k^{th} pierce point, $I^{k}_{Klo,V}$ is the Klobuchar estimate for the k^{th} pierce point, and $d_{k,j}$ is the distance from the k^{th} pierce point to the j^{th} grid point.
Examples of the ionospheric pierce points are shown in Figure 3.

5. Broadcast the grid to the users, via Message Type 26 of the RTCA SC 159 WAAS data format.

6. At the user, estimate the vertical ionospheric delay for each satellite by interpolating between the grid point estimates. This interpolation could use the same routine used by the WMS to find the grid point delays.

7. At the user, convert the vertical delay estimates to slant delays for each satellite.

4 DATA LINK AND FORMAT

Our WMS estimates the ephemeris, clock and ionospheric errors and "packs" them into the RTCA SC 159 WAAS data format as corrections. The total set of defined WAAS message types are shown in Table 1. The table also indicates which messages have been implemented in our current WMS. In many cases, our test messages are slight modifications of the RTCA SC 159 messages. At present, the ionospheric pierce point masks are not sent, because a fixed grid is used for our experimental network.

Our current data link is a cascade of a phone line and a UHF radio, where the radio covers the last mile to the aircraft. More specifically, the radio broadcasts either 2 or 15 Watts at 462.4 MHz, and uses Gaussian Minimum Shift Keying (GMSK) modulation. It operates in broadcast only mode and is not configured for repeat transmission requests. In other words, no acknowledgments are sent from the aircraft to the ground. The radio sends one WAAS message per second. Each message uses 32 bytes or 256 bits, where the last 6 bits are ignored. The broadcast rate is 9600 baud so each message requires only 27 milliseconds to send.

Type	Used	Contents
0	no	Don't use GEO (for testing)
1	yes	PRN mask assignment
2	yes	Fast pseudorange updates
3-8	N/A	Reserved for future messages
9	no	GEO navigation message
10-11	N/A	Reserved for future messages
12	no	WAAS Network/UTC offsets
13-16	N/A	Reserved for future messages
17-22	no	Iono. pierce point masks
23	no	UDRE zone radii and weights
24	no	Mixed term satellite errors
25	yes	Long-term satellite errors
26	yes	Ionospheric delay estimate
27-63	N/A	Reserved for future messages

Table 1 *RTCA SC 159 WAAS message types and an indication of which messages are currently implemented in Stanford's experimental testbed.*

5 AVIONICS

Our airborne equipment is shown in Figure 6. As shown, the WAAS messages are received by the UHF receiver operating at 462.4 MHz. One WAAS message is received each second and passed to the decoding function. The decoding function unpacks the WAAS messages listed in Table 1, and outputs

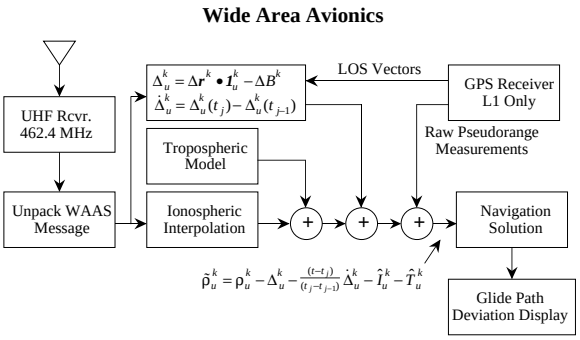

Figure 6 *This schematic shows the components and processes of the user avionics.*

the ionospheric delays, $\{I_\ell^k\}_\ell^{lat,lon}$, and the satellite error components, $\{\Delta r^k, \Delta B^k\}_{k=1}^K$.

The ionospheric grid values are interpolated to yield estimates of the delays at the user's ionospheric pierce points (I_u^k). The tropospheric delays are estimated (T_u^k) using a modified Hopfield model. This model takes no real-time inputs from the WAAS.

The satellite error components are processed as follows to provide pseudorange corrections for each satellite in view of the user

$$\Delta\rho_u^k = \Delta r^k \bullet 1_u^k - \Delta B^k$$

In addition, a corresponding velocity estimate is developed by differencing the last two pseudorange corrections as follows.

$$\Delta\dot{\rho}_u^k = \frac{\Delta\rho_u^k(t_j) - \Delta\rho_u^k(t_{j-1})}{t_j - t_{j-1}}$$

Next, the corrected pseudorange is formed

$$\tilde{\rho}_u^k = \rho_u^k - \Delta\rho_u^k(t_j) - (t - t_j)\Delta\dot{\rho}_u^k - I_u^k - T_u^k$$

These corrected pseudoranges are input to the navigation solution which computes the estimate of the user location. This estimate is fed to another computer which currently houses the glide path computations and display.

The approach guidance was generated by a laptop computer connected to a 5 inch flat panel monitor on the instrument panel. As shown in Figure 7, indications to the pilot were the same as those from a standard ILS: moving needles for horizontal and vertical approach path deviations, marker beacon lights to indicate designated points along the approach, and numerical readouts of height

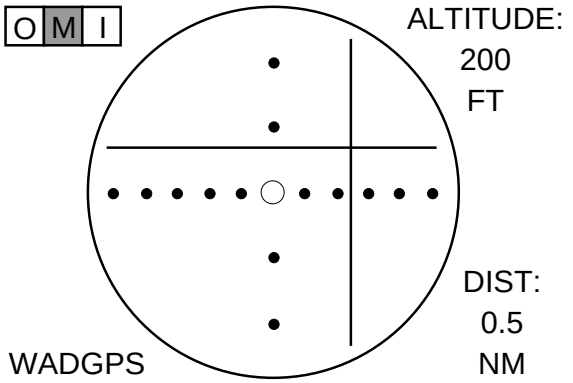

Figure 7 *The WADGPS precision approach guidance display. Here the aircraft is shown to be below and to the left of desired glidepath. The middle marker beacon light is on, indicating aircraft is at 200 feet altitude.*

above runway (in feet) and distance to touchdown (in nautical miles). Localizer needle deflections were based on angular deviation from the localizer beam (6° beamwidth), with the synthetic localizer antenna placed 4800 feet from the touchdown point. The synthetic glideslope antenna was placed 180 feet from the approach end of the runway and generated a 4° glideslope with a 1.4° beamwidth (4° was used instead of the standard 3 because there is a hill off the approach end of the runway). Glideslope needle deflection was based on angular deviation from glidepath until the aircraft was 100 feet above the runway. At this point, the glideslope display was switched from an angular to a linear deviation indicator to eliminate the familiar problem of the ILS glideslope needle becoming overly sensitive just before touchdown. Virtual middle and inner marker beacons were placed under the approach path to indicate that the pilot was passing through altitudes of 200 and 50 feet above the runway. The pilot's display lit up an amber "M" or white "I" when the aircraft flew over these beacons. All antenna locations and needle sensitivities were chosen to accurately reproduce a standard ILS approach.

Antenna locations and glidepath parameters were represented internally in a local coordinate system attached to the runway. This local system was tied in with global XYZ coordinates using a survey of the runway end location and runway direction relative to true north. These are the only two pieces of information required to establish a precision GPS glidepath to a runway.

6 STATIC AND DYNAMIC RESULTS

Two methods have been used to test the accuracies of the generated wide-area differential corrections. The first is to apply the corrections to a

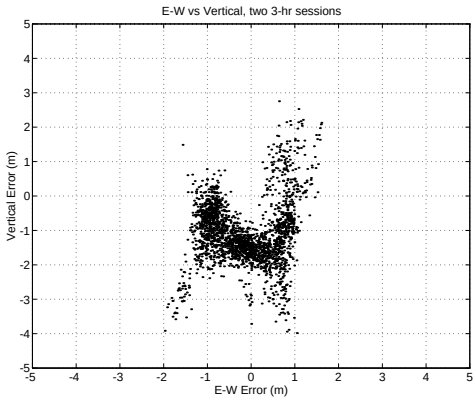

Figure 8 *Here the vertical and horizontal (in the East-West direction) errors are plotted for the afternoon static data sets.*

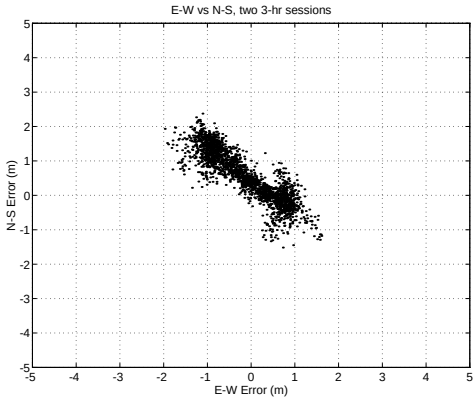

Figure 9 *This plot shows the horizontal errors in both the East-West and North-South directions.*

user at a known static location. The second method is to have the user fly to a surveyed location (such as a runway) and compare the corrected position to the surveyed area. The results of these two tests are described below.

STATIC TESTS

In addition to the three WRSs described in Section 2, we maintain a passive reference station co-located at Stanford with the WMS. The differential corrections derived from the three remote stations are put into RTCA SC 159 format. This message is then "unpacked" and applied to the measurements from the Stanford station. Thus the accuracy of the broadcast corrections can be monitored in real-time.

The locations of the four antennas have been independently measured using standard GPS surveying techniques. The locations have been accurately found in the ITRF-92 reference frame and the relative baselines are self-consistent to the 2 cm level.

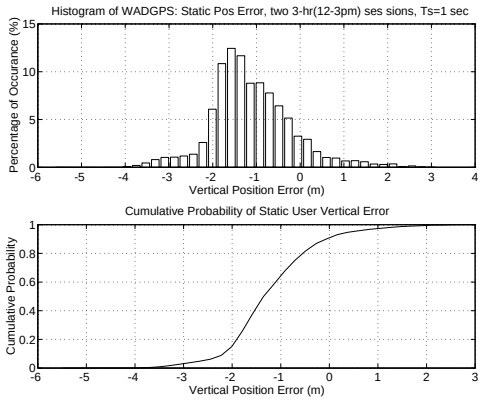

Figure 10 *The distribution of vertical errors for the afternoon static results are shown here.*

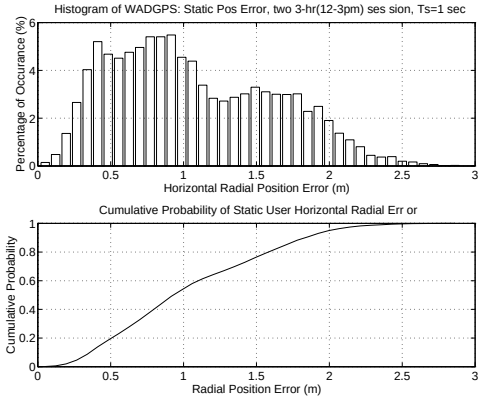

Figure 11 *Here the distribution of circular horizontal errors for the afternoon static results are shown.*

Figures 8 and 9 show the resulting position error at the Stanford station. These plots represent two three hour time periods from the afternoons of two different days. The data was collected during peak ionospheric delay hours, in real-time, at a one hertz rate. Because the corrections are applied at the 250 bps rate there is a resulting latency in the satellite clock corrections of up to six seconds.

Figures 10 and 11 show the distributions of the vertical and horizontal error respectively. For these two periods the mean vertical error is offset 1.1 meters below the true position. The vertical error is contained between -3.1 meters and +1.0 meters 95% of the time. The horizontal error has a mean offset of 0.6 meters and is bounded by 2.0 meters 95% of the time.

Data collected during the nighttime and morning hours are typically more accurate. These results are better than the Category I ILS 95% navigation sensor error limits of ±4.1 meters. As will be shown next, the results are no worse in the dynamic environment.

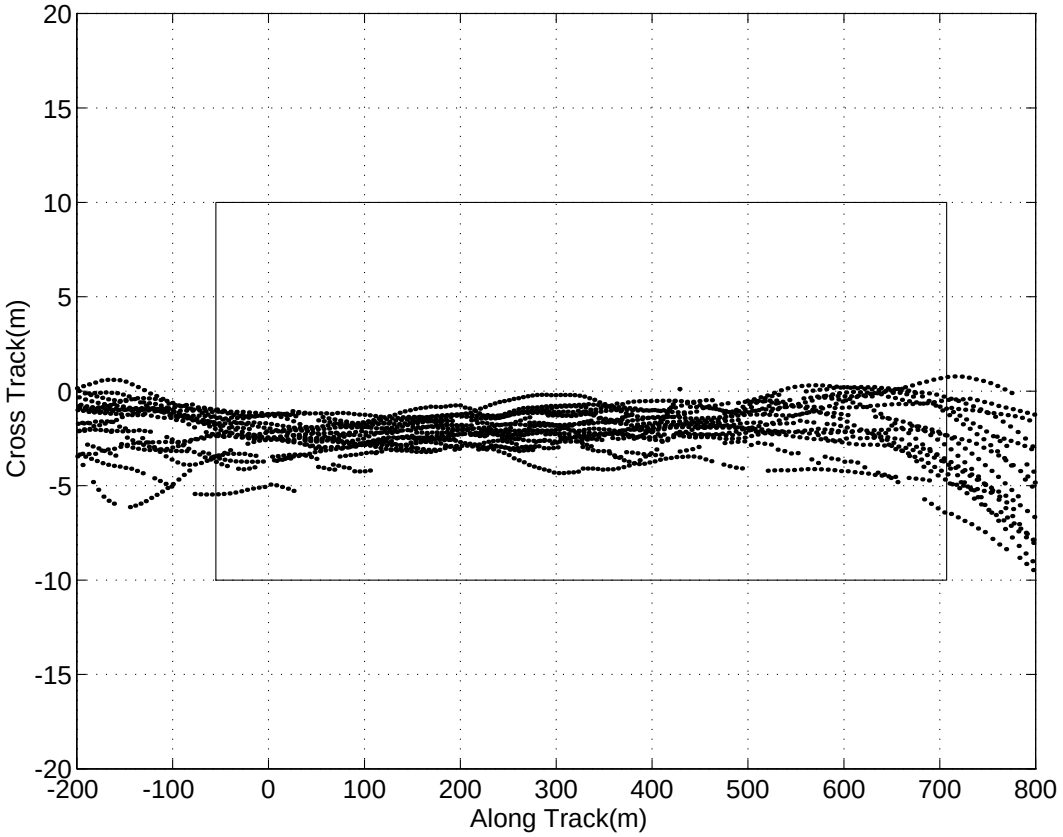

Figure 12 *This plot shows the total system error in the horizontal plane. For reference, the outline of the runway is also shown.*

FLIGHT TRIALS

The flight trials were conducted over several days starting from mid-August 1994. Unfortunately, due to severe problems with our temporary UHF data link, the differential solutions were not always received by the airborne receiver. Consequently, many of the approaches that were flown did not have real-time differential corrections. Fortunately, we did have seventeen approaches, from two different days, in which differential corrections were applied throughout a significant part of each approach. However, because of the data link dropouts, several of these approaches have corrections whose age is in excess of 60 seconds. Despite these less than ideal conditions the results have been outstanding. Figures 12 and 13 summarize these results.

As a truth source we have used the surveyed location of the runway at Palo Alto airport, where we have applied a flat runway model. A previous survey confirms that this approximation should be accurate to better than one meter [13]. The centerline at the desired touch down point of the runway (55 m from the start) is taken as the local origin and the total length of the runway is just over 760 meters.

The horizontal position and the outline of the runway are shown in Figure 12. These points include flight technical error in addition to the navigation sensor error. As is evident from the figure, the total system error is always within 5 meters of the centerline of the runway.

The more important measure, vertical height of the wheels above the runway, is plotted in Figure 13. For each of these landings and take-offs it is safe to assume that the wheels of the airplane were on the runway from roughly 50 meters to 400 meters from the desired touch down point. As a reference the dashed lines show the ±4.1 m 95% error limits for a Category I ILS landing system. It can be seen that, with the exception of one approach, all of the data points are well within these confidence limits.

It is important to note that some of these approaches use pseudorange measurements which have not received differential corrections for more than 30 seconds (in some cases more than 60). In these

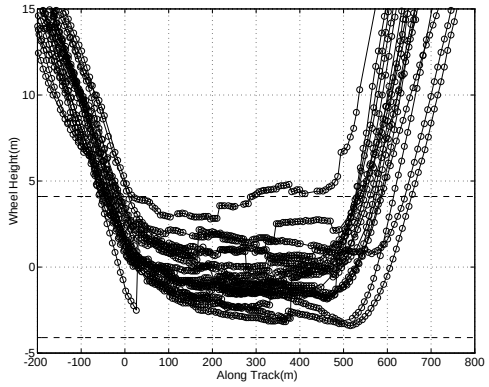

Figure 13 *Here the vertical height of the wheels above the runway are shown. The "jumps" result from satellites with excessively old corrections suddenly receiving new corrections.*

cases the current correction is generated with a simple velocity model from two previous corrections. It is understandable then that the accuracy would be degraded and that the position solution might contain a large "jump" when a new correction finally did arrive.

To give an idea of the capability this system will have with a robust data link, we blindly selected those approaches which did not suffer significant dropouts on final approach. The best six (in terms of data link reliability) are shown in Figure 14. Here the results are remarkably good. Using the runway as truth we find that we are always within two meters of its surveyed height. These are the results we expect to obtain on a routine basis after we have improved the reliability of our data link.

7 Summary and Conclusions

This paper describes an experimental wide-area testbed designed and implemented from scratch by the Wide-Area Differential Laboratory at Stanford University. This network includes three wide-area reference stations located between 300 and 400 miles from Stanford University at Elko, Nevada, San Diego and Arcata, California. It sends the GPS observations over phone lines to a Wide-area Master Station (WMS) on campus. The WMS forms corrections for the ionosphere, satellite ephemeris and satellite clock. These corrections are packed into the RTCA SC 159 WAAS data format and broadcast to Professor David Powell's Piper Dakota. At present, a UHF data link is used, but geostationary satellites will be used in the near future. The WAAS data is applied to the raw pseudoranges measured by a single frequency onboard GPS receiver. The WAAS corrected pseudoranges are used to calculate the aircraft location and glide path deviations. This entire process occurs in real time and yields vertical errors better than 3 meters 95 percent of the time.

ACKNOWLEDGMENTS

The Authors gratefully acknowledge the enormous amount of help and cooperation they have received from: Robin Lampson and Jim Moore at the Elko FAA office, Tom Huber and Curtis Barret at the Montgomery Field FAA office in San Diego and Del Frerret and Tom Bethune at the Arcata FAA office. Their assistance in the installation and maintenance of the three WRSs enabled us to perform this experiment. Special thanks to Jeff Freymueller for processing the antenna survey data.

The authors also gratefully acknowledge the support and assistance of AGS-100 (the satellite program office) especially Joseph Dorfler, Robert Loh and J.C. Johns. Finally we wish to acknowledge all of the help from A.J. Van Dierendonck.

REFERENCES

[1] Department of the Air Force, Interface Control Document ICD-GPS-200-PR, with IRN-200B-PR001, July 1, 1992

[2] M.B. El-Arini, P.A. O'Donnell, P.M. Kellam, J.A. Klobuchar, T.C. Wisser and P.J. Doherty, "The FAA Wide-Area Differential GPS (WADGPS) Static Ionospheric Experiment," Proceedings of the 1993 National Technical Meeting of the Institute of Navigation, San Fransisco, January 1993

[3] M.B. El-Arini, J.A. Klobuchar, P.H. Doherty, "Evaluation of the GPS WAAS Ionospheric Grid Algorithm During the Peak of the Current Solar Cycle," Proceedings of the Institute of Navigation 1994 National Technical Meeting, January 1994

[4] P. Enge, and A.J. Van Dierendonck, "The Wide-Area Augmentation System," Proceedings of the Eighth International Flight Inspection Symposium.

[5] F.M. Haas and M.E. Lage, "GPS Wide-Area Augmentation System (WAAS) Testbed Results - Phase 1D Testbed Results," Proceedings of the Fiftieth Annual Meeting of the Institute of Navigation, Colorado Springs, June 1994

[6] C. Kee, "Wide-Area Differential GPS," PhD. Dissertation, Stanford University, December 1993

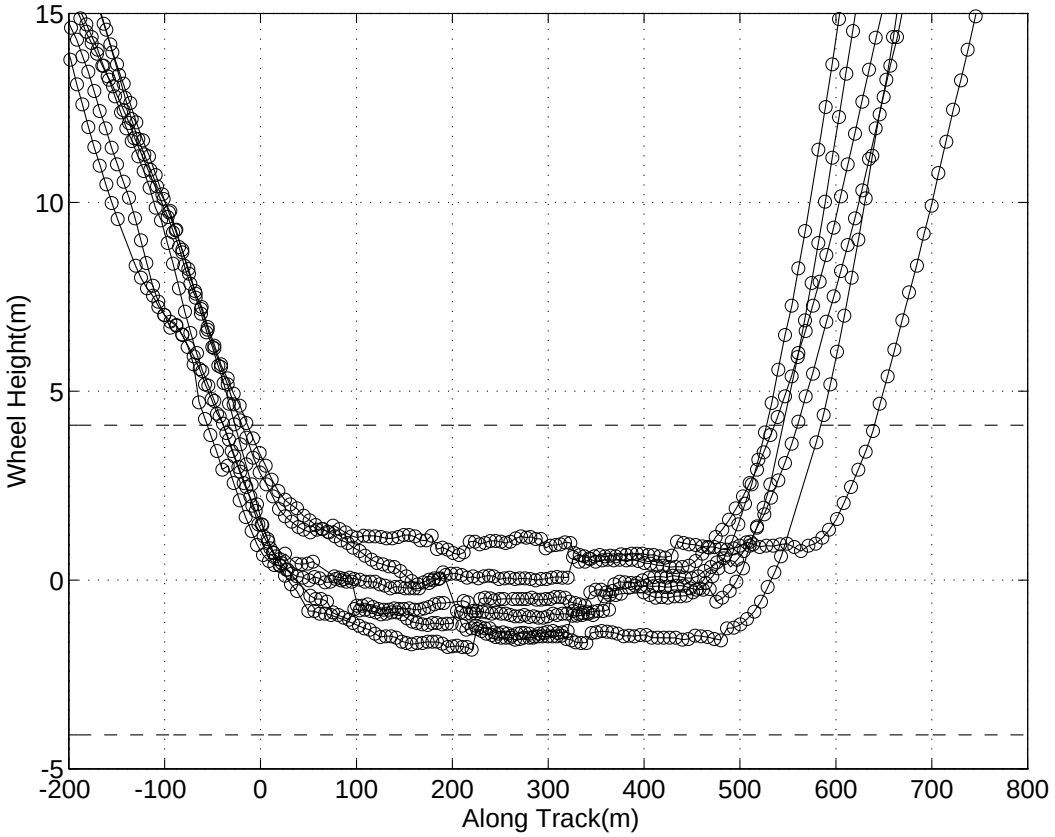

Figure 14 *Here only the approaches which had a solid data link are shown.*

[7] C. Kee and B.W. Parkinson, "High Accuracy GPS Positioning in the Continent: Wide-Area Differential GPS," Proceedings of the Second International Symposium on Differential Satellite Navigation Systems (DNSN93), Amsterdam, March 1993

[8] J.A. Klobuchar, P.H. Doherty, M.B. El-Arini, "Potential Ionospheric Limitations to Wide-Area Differential GPS," Proceedings of the Sixth International Technical Meeting of the Satellite Division of the Institute of Navigation, Sept. 1993

[9] J. Nagle and G.V. Kinal, "Geostationary Repeaters: A Low Cost Way to Enhance Civil User Performance of GPS and Glonass," Record of the IEEE 1990 Position Location and Navigation Symposium, Las Vegas, March 1990

[10] W.S. Phlong and B.D. Elrod, "Availability Characteristics of GPS and Augmentation Alternatives," Proceedings of the 1993 National Technical Meeting of the Institute of Navigation, San Fransisco, January 1993

[11] A.J. Van Dierendonck and P.K. Enge, "The Wide-Area Augmentation System (WAAS) Signal Specification," Proceedings of the Seventh International Technical Meeting of the Satellite Division of the Institute of Navigation, Sept. 1994

[12] V.T. Wullschleger, D.G. O'Laughlin, and F.M. Haas, "FAA Flight Test Results for GPS Wide-Area Augmentation System (WAAS) Cross-Country Demonstration," Proceedings of the Fiftieth Annual Meeting of the Institute of Navigation, Colorado Springs, June 1994

[13] C.E. Cohen, B.S. Pervan, D.G. Lawrence, H.S. Cobb, J.D. Powell and B.W. Parkinson, "Real-Time Flight Test Evaluation of the GPS Marker Beacon Concept for Category III Kinematic GPS Precision Landing," Proceedings of the Annual Meeting of the Satellite Division of the Institute of Navigation (ION GPS-93), Salt Lake City, September 1993.